Resistivity and thermopower calculations in half-Heusler $Ti_{1-x}Sc_xNiSn$ alloys from the KKR-CPA method

2006 J. Phys.: Condens. Matter 18 6379

(http://iopscience.iop.org/0953-8984/18/27/020)

INSTITUTE OF PHYSICS PUBLISHING JOURNAL OF PHYSICS: CONDENSED MATTER

J. Phys.: Condens. Matter **18** (2006) 6379–6389 doi:10.1088/0953-8984/18/27/020

Resistivity and thermopower calculations in half-Heusler $Ti_{1-x}Sc_xNiSn$ alloys from the KKR-CPA method

T Stopa[1], J Tobola[1], S Kaprzyk[1], E K Hlil[2] and D Fruchart[2]

[1] Faculty of Physics and Nuclear Techniques, AGH University of Science and Technology, Aleja Mickiewicza 30, 30-059 Kraków, Poland
[2] Laboratoire de Cristallographie CNRS, 25 Avenue des Martyrs–BP 166, 38042 Grenoble cedex 09, France

Received 27 February 2006, in final form 25 May 2006
Published 23 June 2006
Online at stacks.iop.org/JPhysCM/18/6379

Abstract

The Korringa–Kohn–Rostoker method with the coherent potential approximation (KKR-CPA) was applied to calculate electronic structure and transport coefficients in disordered $Ti_{1-x}Sc_xNiSn$, where semiconductor-to-metal crossovers have recently been observed in resistivity and thermopower experiments (Horyn *et al* 2004 *J. Alloys Compounds* **363** 10; Romaka *et al* 2005 *J. Alloys Compounds* **396** 64). We have investigated the effect of chemical disorder on Fermi surface features (i.e. group velocities and life-times related to real and imaginary parts of complex dispersion curves, respectively). This analysis allowed us to shed light on the principal mechanism responsible for the variation of thermoelectric properties. Using the well-known formulae and performing integration over the complex Fermi surface, the residual conductivity and the thermopower slope S/T were estimated. Satisfying agreement between theoretical results and experimental data (measured at 90 and 300 K) has been found. This may indicate that modifications of electronic structure near E_F are predominantly responsible for the strong decrease of thermopower in $Ti_{1-x}Sc_xNiSn$.

(Some figures in this article are in colour only in the electronic version)

1. Introduction

Heusler X_2YZ phases, where X and Y are transition metal, rare earth or alkaline earth elements and Z represents metalloids (like As, Sn, Sb, Bi), crystallize in the fcc structure (Cu_2MnAl type). When one of the equivalent X sites is empty, the so-called half-Heusler XYZ crystal structure is stabilized (figure 1). These compounds belong to particularly attractive systems, since they exhibit a wide spectrum of remarkable physical properties [3], e.g. half-ferromagnetism, strongly correlated phenomena, localization effects, unusual metal–semiconductor crossovers, etc. It was also established in many electronic structure

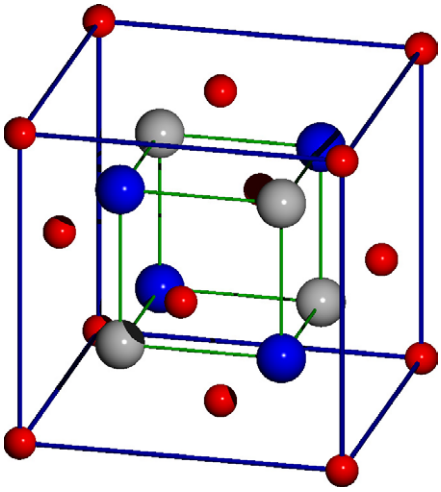

Figure 1. Crystal structure of fcc half-Heusler $Ti_{1-x}Sc_xNiSn$ for $0 < x < 0.6$ ($F\bar{4}3m$, AgMgAs type). Inequivalent atoms: Ni 4a, $(0, 0, 0)$; Sn 4c, $(\frac{1}{4}, \frac{1}{4}, \frac{1}{4})$; and Ti (randomly distributed with Sc atoms) 4d, $(\frac{3}{4}, \frac{3}{4}, \frac{3}{4})$ are plotted by small dark (red), large dark (blue) and large shadow (grey) spheres, respectively (colour on-line).

calculations [4–9] that an energy gap appears above nine valence bands. It was also found that the physical properties of ordered XYZ systems are governed by the number of valence electrons [6, 7]. Hence, many 18-valence electron half-Heusler systems are essentially narrow energy gap semiconductors [10, 11] (unless extra disorder or crystal defects appear [12]) and exhibit large thermopowers [13–15]. The XYZ materials are still considered for potential thermoelectric applications due to wide possibilities of modifying their electronic properties by substitution and doping [16, 17]. Moreover, it has been shown that, by varying alloy composition in systems like Ti(Fe–Ni)Sb [16], Zr(Fe–Pt)Sb or Hf(Fe–Ni)Sb, one can easily control the magnitude and sign of the thermopower, which is also important for obtaining thermocouples.

Recently, a semiconductor-to-metal crossover has been observed in $M_{1-x}Sc_xNiSn$ (M = Ti and Zr) solid solutions from resistivity and thermopower measurements [1]. The semiconducting properties of MNiSn with M = Ti, Zr, Hf have already been well established experimentally [10, 13] and later supported by electronic structure calculations using different methods [4–9, 16].

In the case of the $M_{1-x}Sc_xNiSn$ alloys, the semiconductor-to-metal crossover has recently been interpreted from the computed density of states (DOS) [2]. Here, we have applied the *ab initio* Korringa–Kohn–Rostoker method with coherent potential approximation (KKR-CPA) [19, 20] to study not only the electronic structure of $Ti_{1-x}Sc_xNiSn$ but also the Fermi surface and electron transport properties. It seems that a better understanding of the microscopic mechanisms responsible for electron transport behaviours may help to optimize conditions for efficient thermoelectric devices.

2. Computational details

Electronic structure calculations of parent compounds TiNiSn and ScNiSn (both in cubic and orthorhombic structures) have been performed using the charge and spin self-consistent full-potential KKR method. The crystal potential has been constructed within the local density

approximation (LDA) framework, applying the von Barth–Hedin formula for the exchange–correlation part. With the self-consistent crystal potentials converged up to mRyd, total, site-decomposed and l-decomposed (s, p and d states) DOS have been computed using the tetrahedron integration technique in the reciprocal space. Then, the effects of chemical disorder on the electronic structure in $Ti_{1-x}Sc_xNiSn$ ($0 < x < 0.6$) have been studied employing the KKR-CPA method and within the muffin-tin potential. The charge and CPA cycles have been performed self-consistently on a complex energy contour. The Fermi energy (E_F) for all investigated alloys has been determined from the generalized Lloyd formula [21], which permits us to find E_F precisely from the full derivative of the CPA Green function (without integrating over occupied states). More theoretical details can be found in [19]. For end-point ordered compounds, the muffin-tin KKR-CPA DOS and dispersion curves $E(k)$ were favourably verified by the full-potential KKR computations (see section 3). In all our calculations, experimental crystallographic data were employed.

Following Butler and Stocks' [22] concept of transport coefficient calculations in binary disordered alloys (residual resistivity ρ_0 and thermopower slope S/T extrapolated to $T = 0$ K), we have used the KKR-CPA methodology to calculate the electrical conductivity σ and thermopower S in more complex half-Heusler systems. Earlier, this approach was applied to interpret experimental values of conductivity and thermopower in half-Heusler $TiFe_{1-x}Ni_xSb$, where metal–semiconductor–metal crossovers appeared [18, 23].

The Seebeck coefficient slope can be expressed using the well-known Mott's formula

$$\frac{S}{T} = -\frac{\pi^2}{3}\frac{k_B^2}{e}\frac{\partial \ln \sigma(E)}{\partial E}\bigg|_{E_F}, \tag{1}$$

where the electrical conductivity $\sigma(E)$ can be found from integration over the constant energy surface $\Sigma(E)$:

$$\sigma(E) = \frac{2e^2}{3(2\pi)^3\hbar}\int_{\Sigma(E)} \mathrm{d}S_k v_k \tau_k, \tag{2}$$

where v_k and τ_k correspond to the group velocity and life-time of an electron with wavevector k, respectively. In practical calculations, the energy bands $E(k)$ can be derived from the KKR-CPA method, which are complex values in disordered systems. We extracted these curves, with the effective potential and converged electron charges resulting from the self-consistent procedure. The group velocity of the electron was then determined by numerical differentiation of the real part of $E(k)$:

$$v_k = \frac{1}{\hbar}\nabla_k [\mathrm{Re}\, E(k)] \tag{3}$$

and, from the imaginary part of $E(k)$, the life-time of the electrons was computed:

$$\tau_k = \frac{h}{\mathrm{Im}\, E(k)}. \tag{4}$$

We see, from equations (1) and (2), that the physically interesting energy range, for evaluation of transport coefficients, is mostly the energy bands close to E_F. So, we have to investigate accurately the isoenergy surface shapes, close to E_F, to obtain the energy derivative in equation (1). Note that, from the numerical point of view, the proper extraction of the electron transport coefficients is not always an easy task, since such computations strongly depend on the Fermi surface (FS) complexity. Moreover, it is worth noting that the computational results become unstable when (i) the Fermi level is close to the energy gap, and (ii) the concentration of impurity atoms tends to zero ($x \to 0$). In the first case, the FS is so small that better numerical accuracy is required. In the second case, the decreasing chemical disorder implies a smaller

value of the imaginary part of energy bands and results in unphysically huge values of electron life-times. Consequently, we had to avoid these two cases when calculating the conductivity and thermopower from equations (1) and (2).

3. Results and discussion

3.1. Crystal stability of (Ti–Sc)NiSn system

The half-Heusler TiNiSn (like isoelectronic ZrNiSn and HfNiSn) is a semiconductor with an indirect Γ–X energy gap of order 0.4–0.5 eV, as already reported from many LDA band structure calculations [4, 6, 5, 9, 16]. In this work, we have obtained an energy gap as large as 0.53 eV from the full-potential KKR method for an experimental lattice constant, while a slightly smaller value of $E_g = 0.47$ eV was computed within the muffin-tin approximation. When substituting Ti by scandium in $Ti_{1-x}Sc_xNiSn$, the crystal structure transforms from the cubic AgMgAs type (SG $F\bar{4}3m$) to the orthorhombic TiNiSi type (SG $Pnma$) for $x > 0.6$. To have more insight into the origin of the composition-induced crystal structure transition in $Ti_{1-x}Sc_xNiSn$, electronic structure calculations have been performed for orthorhombic and cubic (hypothetical) phases of ScNiSn. In the case of orthorhombic compounds [24], experimental lattice parameters and atomic positions were employed ($a = 6.625$ Å, $b = 4.333$ Å, $c = 7.536$ Å), Sc 4c: (0.538, 0.25, 0.285); Ni 4c: (0.802, 0.25, 0.569) and Sn 4c: (0.2161, 0.25, 0.592), whereas the extrapolated value of lattice constant ($a = 6.17$ Å) was applied for the cubic compound. Figure 2 shows the total and l-decomposed DOS in both ScNiSn phases. In the cubic compound, one notices an energy gap appearing above the ninth valence band, which is a characteristic feature of the electronic structure of many half-Heusler systems. The Fermi level falls into a strongly decreasing DOS slope with an important value of $n(E_F)$ (mainly due to d-states on transition element atoms) but insufficient to satisfy the Stoner limit (see figure 3). Indeed, the spin-polarized KKR-CPA calculations confirmed the non-magnetic ground state of $Ti_{1-x}Sc_xNiSn$.

In the orthorhombic ScNiSn, valence bands are visibly wider, most likely due to smaller interatomic distances and stronger hybridization among transition elements' d-states and Sn p-states. This results in a DOS valley in the vicinity of E_F with a value of $n(E_F) = 9.6$ states/Ryd/spin per fu, which is almost three times smaller than the value computed in cubic ScNiSn (26.2 states/Ry/spin per fu). This finite DOS value at E_F found in orthorhombic ScNiSn corresponds well to the metallic-like character of the measured electrical resistivity [24]. The electronic structure behaviour detected in two forms of ScNiSn, i.e. the DOS valley in the vicinity of E_F in orthorhombic compound (figure 2) against the strong increase in the DOS near E_F in the cubic zone when substituting Ti with Sc (figure 3), may tentatively support the crystal structure transition observed in $Ti_{1-x}Sc_xNiSn$ alloy [1, 2].

Furthermore, we performed total energy calculations with the full-potential KKR method for end compounds, both in cubic and orthorhombic phases. The obtained results are shown in table 1. One can notice that these energy values are in agreement with the experimental observation that TiNiSn crystallizes in the half-Heusler structure while ScNiSn prefers the orthorhombic structure. More quantitative analysis of the crystal structure change would require the comparative total energy KKR-CPA calculations of $Ti_{1-x}Sc_xNiSn$, near content of $x = 0.6$, both in orthorhombic and cubic phases, but we are not aware of crystallographic data in orthorhombic solid solutions.

3.2. Electron transport parameters in $Ti_{1-x}Sc_xNiSn$ system

In order to investigate the FS evolution versus alloy composition, KKR-CPA calculations have been performed for $Ti_{1-x}Sc_xNiSn$ at experimental contents, i.e. $x = 0.05$, 0.1, 0.2, 0.3, 0.4,

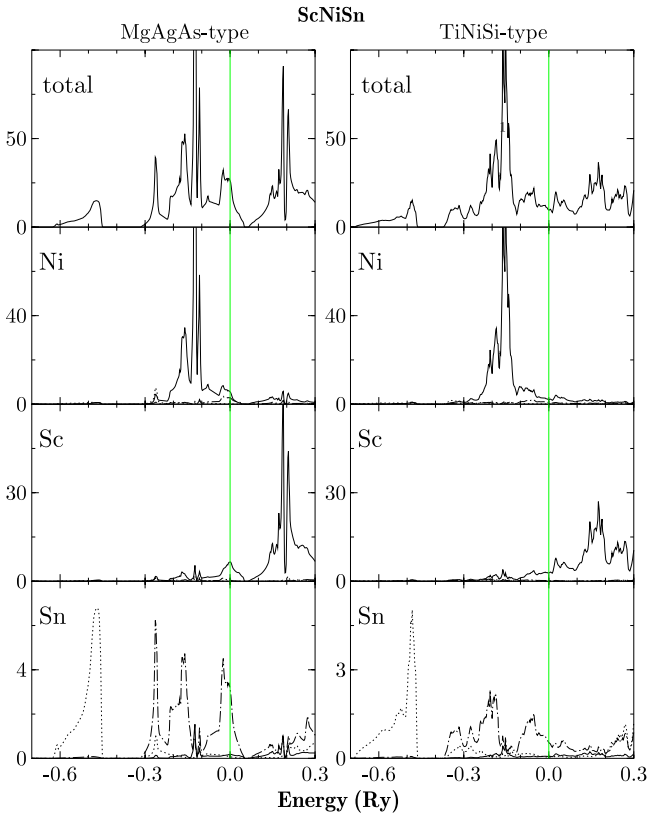

Figure 2. KKR total (top panels) and partial density of states (DOS) in orthorhombic TiNiSi-type (right column) and cubic MgAgAs-type (hypothetical) ScNiSn. In the lower panels, s-, p- and d-DOS are plotted by dot, dot–dashed and solid lines, respectively.

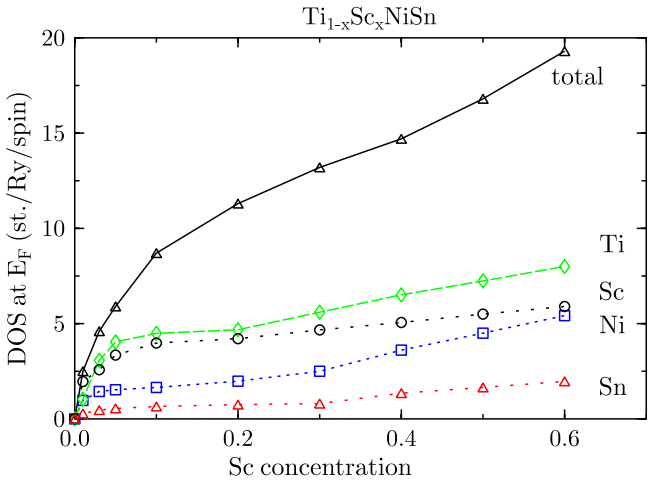

Figure 3. Total and site-decomposed DOS at the Fermi level in half-Heusler $Ti_{1-x}Sc_xNiSn$.

0.5 and 0.6. Since the electronic structure of $M_{1-x}Sc_xNiSn$ (M = Ti and Zr) has recently been reported in detail [2], we only present the variation of total and site-decomposed DOS at

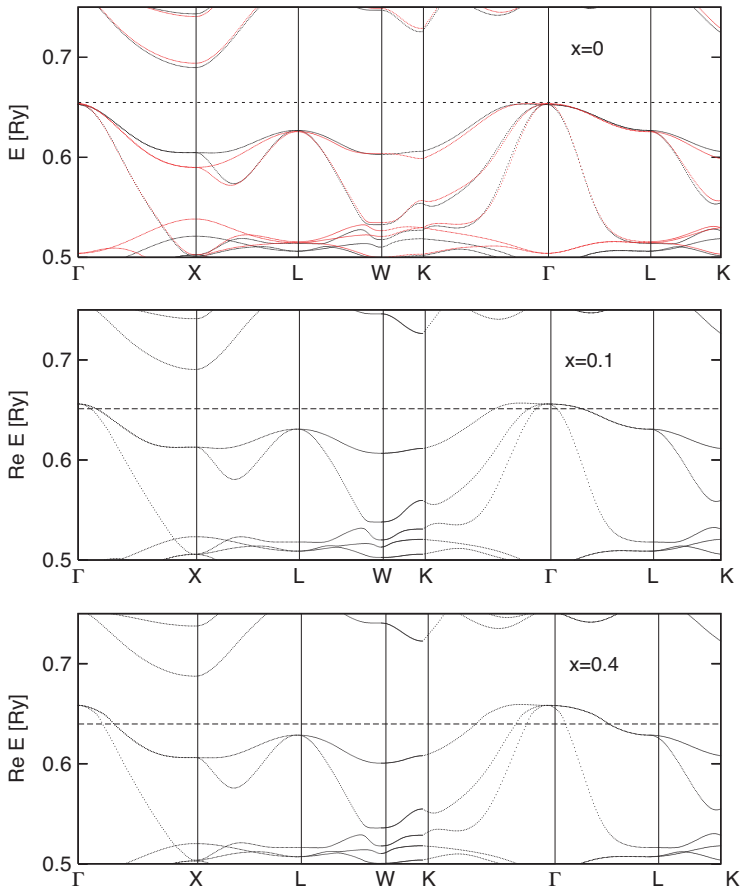

Figure 4. Dispersion curves $E(k)$ in the vicinity of E_F (marked by a horizontal dashed line) along high symmetry directions in selected compositions of half-Heusler $Ti_{1-x}Sc_xNiSn$. The upper panel shows the $x = 0$ limit. Full potential and muffin-tin KKR results are plotted by red and black lines, respectively. In the picture, the E_F value for the full-potential case was translated to E_F found for the muffin-tin approximation. Lower panels show KKR-CPA bands for $x = 0.1$ and 0.4. The Fermi level cuts three valence bands (seen along the Γ–X direction) (colour on-line).

Table 1. Full-potential KKR total energies for TiNiSn and ScNiSn calculated for both cubic ($F\bar{4}3m$) and orthorhombic ($Pnma$) structures. $\Delta E = E(F\bar{4}3m)–E(Pnma)$.

Compound	$E(F\bar{4}3m)$	$E(Pnma)$	ΔE
TiNiSn	−68 354.612 Ryd	−68 354.272 Ryd	−0.340 Ryd
ScNiSn	−67 638.632 Ryd	−67 638.864 Ryd	+0.232 Ryd

E_F in $Ti_{1-x}Sc_xNiSn$ versus Sc content (figure 3). The total as well as the transition metals' contributions to $n(E_F)$ strongly increases with Sc content, especially at low x. One can also notice that Ti d-states mainly contribute to the DOS near the valence band edge (for small x), but Ni d-states are also important and they increase with x, being comparable to those of Ti and Sc for $x > 0.4$. In Ti-rich $Ti_{1-x}Sc_xNiSn$ compounds, the Fermi level crosses three valence bands in the vicinity of the Brillouin zone (BZ) centre. This can be observed on plots (figure 4) of the real part of complex dispersion curves $E(k)$ along high symmetry directions. In order

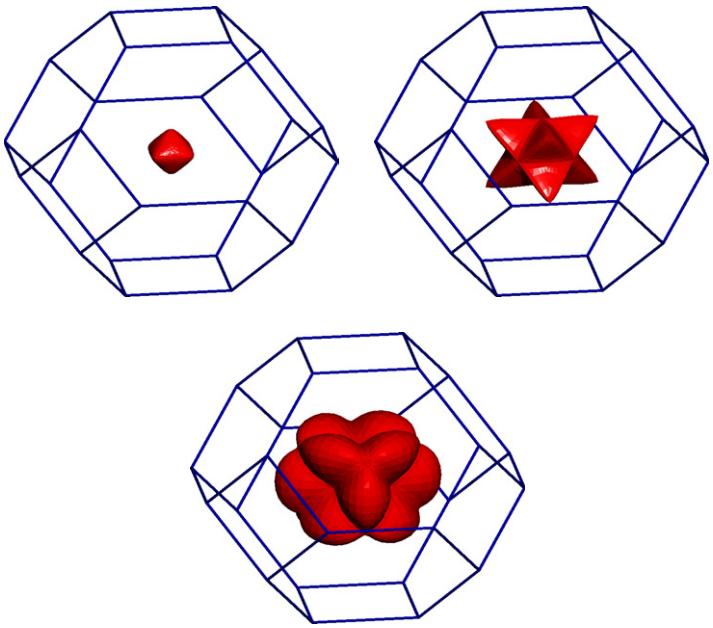

Figure 5. KKR-CPA Fermi surface (FS) in disordered half-Heusler $Ti_{0.7}Sc_{0.3}NiSn$. The FS consists of the three FS sheets, shown in the subsequent pictures.

to investigate the effect of the muffin-tin approximation on energy bands, we compared our results with full-potential calculations for TiNiSn ($x = 0$), as shown in the upper panel of figure 4. We see that the bands close to the bottom of the energy gap are very similar in both these cases. Hence, one supposes that the muffin-tin approximation is sufficiently accurate to evaluate electron transport properties in the $Ti_{1-x}Sc_xNiSn$ alloys. The differences between both methods are bigger for the other parts of the dispersion curves.

Figure 5 illustrates the whole Fermi surface for $x = 0.3$ composition, which consists of three sheets, as presented in the separate pictures in figure 5. The evolution of the Fermi surface can be seen better in figure 6, where FS cross-sections are projected on the k_x–k_y plane. In this figure, the three FS sheets are displayed. The innermost sheet has the shape of an octahedron and is not connected with the other two sheets. The second and third sheets are strongly aspherical and are connected with each other along selected high-symmetry directions in the BZ, due to double band degeneracy. Interestingly, one can observe precisely in figure 6 that the FS area increases with Sc concentration up to about $x = 0.5$ and again decreases for $x = 0.6$. This FS phenomenon is probably related to the crystal structure transition occurring in $Ti_{1-x}Sc_xNiSn$ at about $x = 0.6$. Figures 7 and 8 present the average values of electron group velocities (derived from equation (3)) and life-times (from equation (4)) obtained from integration over all FS sheets.

On the whole, one can note that group velocities and life-times behave in a particular way and that there are some concentration-dependent correlations between the calculated transport parameters, e.g. the electron velocity decreases when the electron life-time increases. Moreover, for $x = 0.4$, a minimum electron life-time (due to chemical disorder) of order 10^{-10} s can be observed. This minimum corresponds to the maximum of the computed electron velocities being as large as 0.5×10^6 m s^{-1}. As can be expected from the curvature of the FS (figure 6), the largest contribution to the average velocity comes from electrons with k-vectors on the first FS sheet.

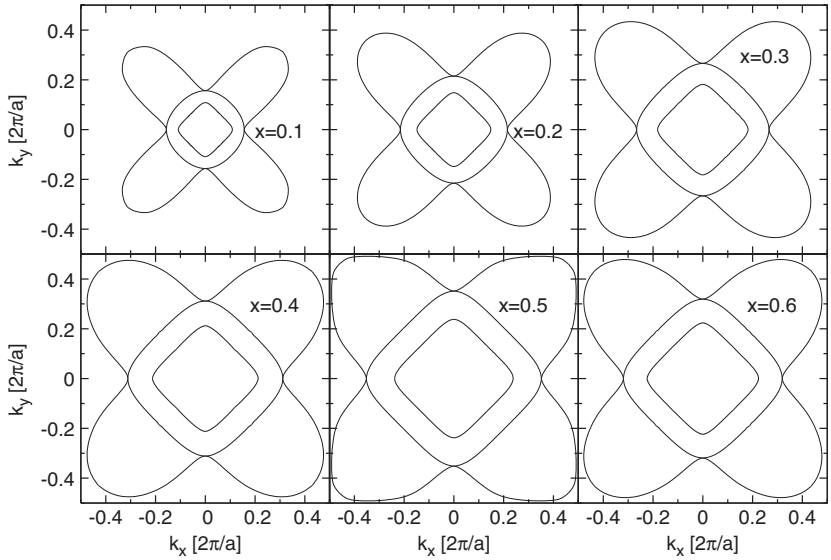

Figure 6. The evolution of FS cross-sections along the k_x–k_y plane in half-Heusler $Ti_{1-x}Sc_xNiSn$.

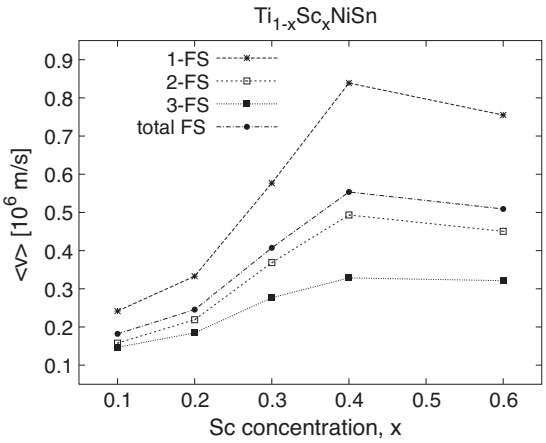

Figure 7. Electron group velocity calculated for three FS sheets in $Ti_{1-x}Sc_xNiSn$.

3.3. Resistivity and thermopower

The residual resistivity in $Ti_{1-x}Sc_xNiSn$, calculated from equation (2), strongly decreases with Sc content (figure 9), which supports well the experimental observation of a semiconductor-to-metal crossover [2]. The obtained KKR-CPA values of electrical resistivity cannot be compared directly with the measured points, since the experimental curves were collected in the 80–300 K temperature range [1, 2], where electron–phonon scattering should be taken into account. Conversely, one can try to compare experimental data with the thermopower estimated from the S/T slope (computed from equations (1) and (2)) if accounting for only the linear term of the the Seebeck coefficient. In general, one can express the thermopower as $S(T) = AT + BT^3 + \cdots$, where at low temperature the linear term $AT = (S/T)_{T=0}T$

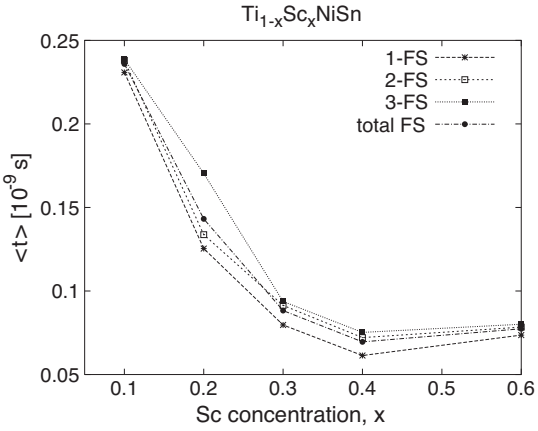

Figure 8. Electron life-times calculated in $Ti_{1-x}Sc_xNiSn$.

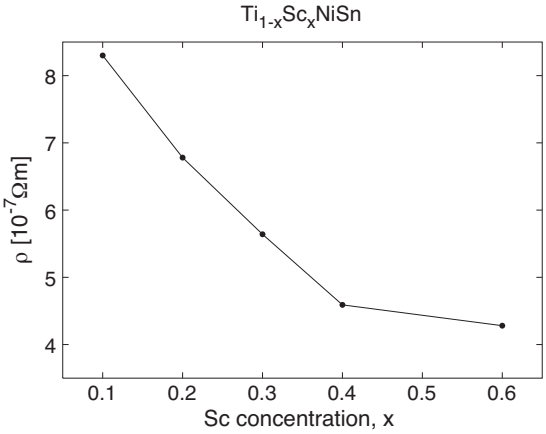

Figure 9. KKR-CPA residual resistivities computed in $Ti_{1-x}Sc_xNiSn$.

Table 2. Comparison of measured [1, 2] and KKR-CPA calculated thermopower for $T = 90$ and 300 K in half-Heusler $Ti_{1-x}Sc_xNiSn$.

Composition	$S_{exp}^{90\,K}$	$S_{calc}^{90\,K}$	$S_{exp}^{300\,K}$	$S_{calc}^{300\,K}$
$Ti_{0.9}Sc_{0.1}NiSn$	29.8	30.3	94.4	100.6
$Ti_{0.8}Sc_{0.2}NiSn$	12.6	15.3	60.5	51.1
$Ti_{0.7}Sc_{0.3}NiSn$	4.6	10.0	33.4	36.5
$Ti_{0.6}Sc_{0.4}NiSn$	4.0	3.1	16.7	10.2
$Ti_{0.4}Sc_{0.6}NiSn$	−0.4	0.6	7.1	2.1

should be dominant when electrical conductivity is mostly related to chemical disorder. The experimental points (measured at 90 and 300 K [1, 2]) and the computed values of the Seebeck coefficients are compared in table 2. We observe that, quantitatively, KKR-CPA calculations reflect well the thermopower decrease in $Ti_{1-x}Sc_xNiSn$ with increasing Sc concentration. Good agreement between experimental and theoretical thermopower is illustrated in figure 10, where theoretical and experimental points gained at 300 K are plotted.

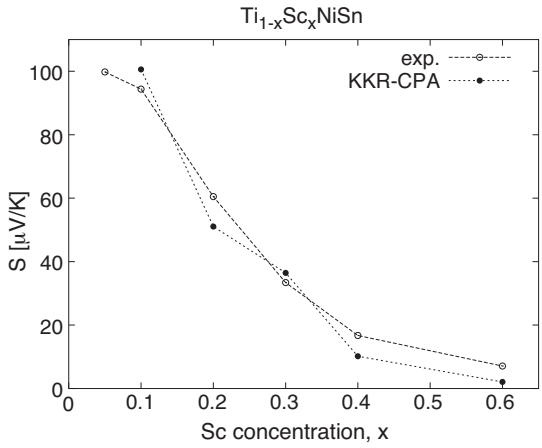

Figure 10. Room-temperature Seebeck coefficient in $Ti_{1-x}Sc_xNiSn$. Experimental and theoretical (see text) points are marked by open and solid circles, respectively. Lines are only guides for the eye.

One could try to perform a more simplified analysis of the low-temperature thermopower slope based exclusively on variation of total DOS near the Fermi level. In this case, the kinetic parameters of electrons, such as group velocity and life-time, are not taken into account when calculating σ. Assuming that residual electrical conductivity $\sigma(E)$ is proportional to the density of states $n(E)$ and that carrier mobility $\mu(E)$ slowly varies with energy ($\approx$constant), i.e. $\sigma(E) \propto n(E)\mu_0$, the thermopower can be derived using equation (1) from the expression: $S/T = -2.877 \times 10^{-2}\,\mathrm{d}\ln n(E)/\mathrm{d}E$. In this formula, S/T is expressed in V K^{-2} and $n(E)$ in states/Ryd/fu. When energy is measured in Rydbergs, we obtained the following values of S/T (in μV K^{-2}): 0.356, 0.278, 0.122 and 0.088 for $x = 0.1, 0.20.4$ and 0.6, respectively. At temperature $T = 90$ K, these values resulted in the corresponding Seebeck coefficients (in μV K^{-1}): 32, 25, 11 and 8, which reproduce relatively well the thermopower variations observed in experimental measurements. Nevertheless, it seems that such a rough analysis tends to overestimate the calculated thermopower in the investigated alloys and should rather be used in a qualitative discussion of electron transport properties.

4. Conclusions

We have calculated the electronic structure of $Ti_{1-x}Sc_xNiSn$ half-Heusler systems using the muffin-tin KKR-CPA method as well as the full-potential KKR technique for parent compounds TiNiSn and ScNiSn. Upon substitution of Ti with Sc, the Fermi level shifts in a systematic way from an energy gap in pure TiNiSn to valence states in disordered $Ti_{1-x}Sc_xNiSn$. This behaviour corresponds well to the experimental findings [1, 2], revealing a decrease in the absolute values of both resistivity and hole-like thermopower when the Sc content increases. From the KKR-CPA calculations of complex energy bands, group velocities and life-times of electrons on the Fermi surface were then derived. This allowed the determination of the composition dependence of the residual conductivity and thermopower slope. The theoretical values of the Seebeck coefficient obtained from the linear extrapolation of S/T to finite temperatures remain in satisfying agreement with experimental data. Our results confirm that electron transport properties in $Ti_{1-x}Sc_xNiSn$, which is near to the semiconductor–metal limit, are dominated by chemical disorder.

In summary, the reasonable agreement of our calculations with experimental data in the half-Heusler systems gives us confidence that KKR-CPA theory may be suitable for studying thermoelectric properties in more complex disordered alloys.

Acknowledgments

This work was partly supported by the French–Polish project Polonium 2006–2007, as well as the Polish State Committee for Scientific Research (KBN) grant No. 1P03B 162 29. We also thank Professor L Romaka for sending numerical data of electrical resistivity and thermopower measurements in half-Heusler $Ti_{1-x}Sc_xNiSn$.

References

[1] Horyn A, Bodak O, Romaka L, Gorelenko Yu, Tkachuk A, Davydov V and Stadnyk Yu 2004 *J. Alloys Compounds* **363** 10
[2] Romaka L, Stadnyk Yu, Horyn A, Shelyapina M G, Kasperovich V S, Fruchart D, Hlil E K and Wolfers P 2005 *J. Alloys Compounds* **396** 64
[3] Pierre J, Skolozdra R V, Tobola J, Kaprzyk S, Hordequin C, Kouacou M A, Karla I, Currat R and Lelievre-Berna E 1997 *J. Alloys Compounds* **262/263** 101
[4] Ogut S and Rabe K M 1995 *Phys. Rev.* B **51** 10443
[5] Slebarski A, Jezierski A, Zygmunt A, Mahl S and Neumann M 1998 *Phys. Rev.* B **57** 9544
[6] Tobola J, Pierre J, Kaprzyk S, Skolozdra R V and Kouacou M 1998 *J. Phys.: Condens. Matter* **10** 1013
[7] Tobola J and Pierre J 2000 *J. Alloys Compounds* **296** 243
[8] Larson P, Mahanti S D and Kanatzidis M G 2000 *Phys. Rev.* B **62** 12754
[9] Galanakis I, Dederichs P H and Papanikolaou N 2002 *Phys. Rev.* B **66** 134428
[10] Aliev F G, Brandt N, Moshchalkov V V, Kozyrkov V V, Skolozdra R V and Belogorokhov A I 1989 *Z. Phys.* B **75** 167
[11] Kouacou M A, Pierre J and Skolozdra RV 1995 *J. Phys.: Condens. Matter* **7** 7373
[12] Jodin L, Tobola J, Pecheur P and Scherrer H 2004 *Phys. Rev.* B **70** 184207
[13] Uher C, Yang J and Hu S 1999 *Phys. Rev.* B **59** 8615
[14] Hohl H, Ramirez A P, Goldmann C, Ernst G, Wolfling B and Bucher E 1999 *J. Phys.: Condens. Matter* **11** 1697
[15] Poon S J 2001 *Semicond. Semimet.* **70** 37
[16] Chaput L, Tobola J, Pecheur P and Scherrer H 2006 *Phys. Rev.* B **73** 045121
[17] Sakurada S and Shutoh N 2005 *Appl. Phys. Lett.* **86** 082105
[18] Tobola J, Jodin L, Pecheur P, Scherrer H, Venturini G, Malaman B and Kaprzyk S 2001 *Phys. Rev.* B **64** 155103
[19] Bansil A, Kaprzyk S, Mijnarends P E and Tobola J 1999 *Phys. Rev.* B **60** 13396
[20] Stopa T, Kaprzyk S and Tobola J 2004 *J. Phys.: Condens. Matter* **16** 4921
[21] Kaprzyk S and Bansil A 1990 *Phys. Rev.* B **42** 7358
[22] Butler W H and Stocks G 1984 *Phys. Rev.* B **29** 4217
[23] Stopa T, Tobola J and Kaprzyk S 2004 *Proc. 2nd European Conf. on Thermoelectrics (Krakow, Poland, Sept. 2004)*
[24] Kotur B Ya and Kalychak I P 1989 *IANSSSR Neorgan. Mater.* **25** 597